



Effects of doping zinc oxide nanoparticles with transition metals (Ag, Cu, Mn) on photocatalytic degradation of Direct Blue 15 dye under UV and visible light irradiation

Roya Ebrahimi¹ · Khosro Hossienzadeh¹ · Afshin Maleki¹ · Reza Ghanbari² · Reza Rezaee¹ · Mahdi Safari¹ · Behzad Shahmoradi¹ · Hiua Daraei¹ · Ali Jafari³ · Kaan Yetilmezsoy⁴ · Shivaraju Harikaranahalli Puttaiah⁵

Received: 22 October 2018 / Accepted: 11 March 2019 / Published online: 1 April 2019

© Springer Nature Switzerland AG 2019

Abstract

Background Azo dyes represent the most commonly used group of dyes in the textile industry. These organic dyes are mainly resistant to biodegradation and may exhibit toxic and carcinogenic properties. The purpose of this study was to investigate the effects of doping zinc oxide (ZnO) nanoparticles (NPs) with transition metals (silver, manganese, and copper) on the photocatalytic efficiency of ZnO NPs in the removal of Direct Blue 15 dye from aqueous environments under ultraviolet (UV) radiation and visible light irradiation.

Methods One or two metals were used for doping the NPs. In total, seven types of undoped and transition metal-doped NPs were synthesized using the thermal solvent method with ZnO precursors and transition metal salts. The characteristics of the synthesized NPs were determined based on the scanning electron microscopy (SEM), energy-dispersive X-ray spectroscopy (EDX), X-ray diffraction (XRD), Fourier transform infrared (FTIR) spectroscopy, dynamic light scattering (DLS), atomic force microscopy (AFM), and zeta potential measurements.

Results The produced ZnO NPs did not exhibit any particular photocatalytic activities under UV radiation and visible light irradiation. The highest removal efficiency under UV radiation was about 74% in the presence of silver-doped ZnO NPs, while the maximum efficiency under visible light was 70% in the presence of copper-doped ZnO NPs. The lowest removal efficiency

Highlights

- Transition metal-doped ZnO NPs was used for photocatalytic removal of Direct Blue 15 dye.
- Photocatalytic activity of ZnO NPs was improved after doping with Ag, Mn, and Cu.
- SEM, XRD, FTIR, and AFM corroborated the synthesis of transition metal-doped NPs.
- Photocatalysis using Ag-doped ZnO NPs could degrade 74% of dye under UV radiation.
- About 70% of dye could be removed using Cu-doped ZnO NPs under visible light.

✉ Afshin Maleki
maleki43@yahoo.com; malaki@muk.ac.ir

✉ Kaan Yetilmezsoy
yetilmez@yildiz.edu.tr; kyetilmezsoy@gmail.com

Roya Ebrahimi
ebrahimi83@yahoo.com

Khosro Hossienzadeh
khosrohossienzadeh1362@gmail.com

Reza Ghanbari
r.ghanbari@qums.ac.ir

Reza Rezaee
rezaee.eng@gmail.com

Mahdi Safari
safari.m.eng@gmail.com

Behzad Shahmoradi
bshahmorady@gmail.com

Hiua Daraei
hiua.daraei@gmail.com

Ali Jafari
jafari_a99@yahoo.com

Shivaraju Harikaranahalli Puttaiah
shivarajuenvi@gmail.com

Extended author information available on the last page of the article

was related to pure ZnO, which was 18.4% and 14.6% under UV and visible light irradiation, respectively. Although the efficiency of dye removal under visible light was not high compared to UV radiation, this efficiency was noteworthy in terms of both practical and economic aspects since it was achieved without the presence of ultraviolet radiation.

Conclusions The synthesis of transition metal-doped ZnO nanophotocatalysts (with one or two metals) under UV radiation or visible light irradiation could be used as an efficient and promising technology for the photocatalytic removal of Direct Blue 15 dye from aqueous environments.

Keywords Direct Blue 15 · Doping · Photocatalytic removal · Transition metals · Zinc oxide nanoparticles

Abbreviations

AFM	Atomic Force Microscopy
AOP	Advanced Oxidation Processes
CAS	Chemical Abstracts Service
CB	Conduction Band
DLS	Dynamic Light Scattering
EC	European Community
EDX	Energy-Dispersive X-ray Spectroscopy
ELS	Electrophoretic Light Scattering
FTIR	Fourier Transform Infrared Spectroscopy
NPs	Nanoparticles
PALS	Phase Analysis Light Scattering
SEM	Scanning Electron Microscopy
UV	Ultraviolet
VB	Valence Band
XRD	X-ray Diffraction

Background

The waste of textile industries contains high levels of organic pollutants such as dyeing materials. Untreated discharge of this waste into receiving waters is a major source of environmental pollution worldwide [1]. Azo dyes are one of the most widely used dye compounds in textile industries accounting for 60% to 70% of the total used textile dye around the world [2]. These dyes, which are characterized by nitrogen-nitrogen double bonds (-N=N-) in their structure, are responsible for color formation, together with other chromophores [3].

According to the results of previous studies, nearly 15–20% of the total produced textile dye around the world is discharged into wastewater during dyeing processes. The presence of these compounds in water is noticeable, even at very low concentrations (< 1 mg/L), and negatively acts upon the quality of water [4]. Besides color formation, these dyeing compounds can affect environmental aesthetics. In addition, through reducing light penetration in water, they influence the photosynthetic activities of plants, reduce the content of dissolved oxygen in water, increase the level of suspended solids and turbidity, and finally increase organic loading in the aquatic environment. On the other hand, many dyeing compounds are resistant to biological degradation and oxidizing agents due to the presence of aromatic compounds in their molecular structure. Consequently, they are

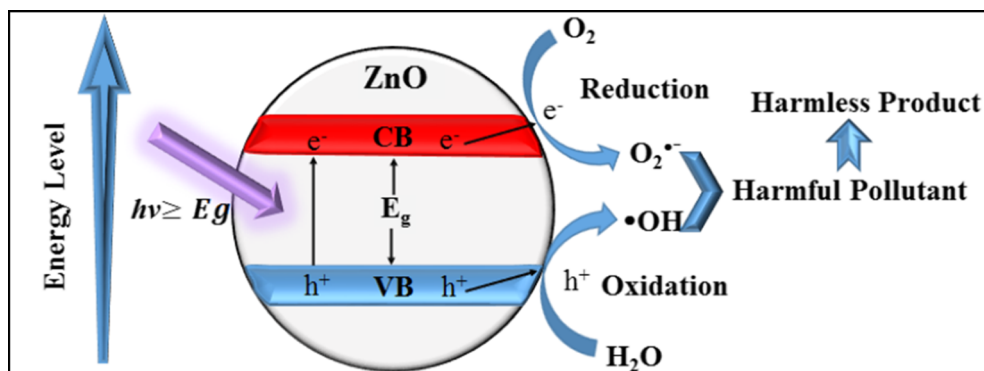
carcinogenic and toxic to humans and aquatic organisms [5–8]. To reduce the harmful effects of these pollutants on the environment, it is necessary to remove them from wastewater prior to discharging into the environment [9, 10].

The conventional physical and chemical methods of wastewater treatment, including coagulation, flocculation, filtration, adsorption, and chlorination, cannot completely degrade or mineralize organic pollutants. Also, changes in the phase of these pollutants from liquid to solid and occasional formation of transition metal complexes (due to decomposition) create a number of other problems in this area, which require more refinement and investment [11, 12]. According to the recent literature, advanced oxidation processes (AOP), especially photocatalytic methods, are effective and efficient in the treatment of industrial wastewater. The efficiency of these methods is attributed to the production of active species, such as hydroxyl radicals ($\bullet\text{OH}$), for decomposing pollutants, which are resistant to simple and harmless substances (e.g., water and carbon dioxide) [13–15].

Photocatalytic reactions occur as a result of ultraviolet (UV) or visible light irradiation on the surface of a semiconductor catalyst (e.g., TiO_2 and ZnO). These reactions can excite electrons from the valence band and transfer them to the conduction band. The generated hole-electron (h/e) pair at the catalyst level oxidizes pollutant molecules by producing more hydroxyl radicals and participating in oxidation and regeneration reactions [16–18]. Figure 1 presents the oxidation mechanism of organic pollutants in a nanophotocatalytic process. Overall, selection of a suitable catalyst is of great significance, as the optical activity of semiconductor catalysts depends on their capacity to absorb light and generate hole-electron pairs and hydroxyl radicals [19, 20].

In recent studies, special attention has been paid to zinc oxide (ZnO) nanoparticles (NPs) as semiconductor catalysts with important properties, such as high chemical stability, nontoxicity, great optical and electrical properties, and high oxidizing potential. These NPs have been used for decomposition and oxidation of resistant organic pollutants [21]. However, considering the wide band gap (3.37 eV), ZnO shows photocatalytic activity only under UV light [22], which constitutes 5% to 7% of the solar energy. Therefore, use of sunlight as a natural source is limited for this purpose. Additionally, rapid recombination of hole-electron pairs is another limitation of ZnO NPs [23].

Fig. 1 The photocatalytic processes of contaminant oxidation [21]



Generally, it is necessary to overcome the limitations of photocatalysts to improve their performance and practical application. One of the methods, which has recently attracted the researchers' attention, is doping of ZnO NPs with transition metals, such as manganese (Mn), silver (Ag), iron (Fe), gold (Au), and copper (Cu) [24]. Doping of ZnO with an appropriate dopant can change its bandgap energy and prevent recombination of charge carriers (electron-hole pairs), which promote its efficiency in photocatalytic and sonocatalytic degradation of organic and toxic pollutants [25–27]. Since the state and reduction energy level of many transition metals lies within the bandgap energy of ZnO, doping a transition metal ion into ZnO structures generates new electronic levels from the conduction band (CB) to the valence band (VB) of ZnO. The generation of such levels enables absorption of visible light and charge transition from the d-orbital of the dopant to the CB or VB of ZnO [28]. Metal ions act as a trap for the produced light electrons by penetrating into the ZnO structure, and prevent the rapid hole-electron recombination, resulting in the increased photocatalytic activity of doped NPs, compared to their undoped counterpart [19].

In this regard, in a study by Kumar et al. [29], Cu-doped ZnO exhibited high optical absorption and considerable photocatalytic activity in decomposition of Red Direct dyes. In another study, Chang et al. [30] examined the light absorption capacity, hole-electron pair separation, and photocatalytic efficacy of cerium-doped ZnO NPs and reported photocatalytic improvements. With this background in mind, the purpose of the present study was to investigate the efficiency of doping ZnO NPs with transition metals, including Ag, Mn, and Cu (both as single and paired metals), in removing Direct Blue 15 dye under UV and visible light irradiation in the laboratory.

Materials and methods

Chemicals

The dye used in this study was Direct Blue 15 ($C_{34}H_{24}N_6O_{16}S_4Na_4$) and was purchased from Alvan

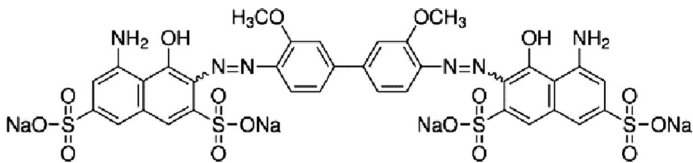
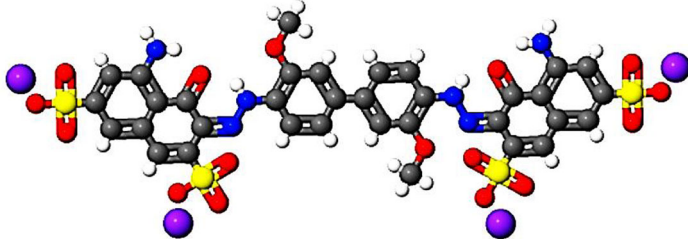
Sabet Company (Iran). Structural and some physicochemical characteristic of Direct Blue 15 dye are presented in Table 1. Merck Company (Darmstadt, Germany) supplied other chemicals, including silver nitrate ($AgNO_3$), manganese acetate ($Mn(CH_3COO)_2 \cdot 4H_2O$), and copper acetate ($Cu(CH_3COO)_2$), which were used as precursors for the synthesis of Ag-, Mn-, and Cu-doped ZnO NPs, respectively. Zinc nitrate hexahydrate (99%) and oxalic acid (99%) were also purchased from Merck for the process of synthesis.

Synthesis of nanoparticles

The thermal solvent method was used to synthesize undoped ZnO nanocatalysts, as well as doped ZnO nanoparticles (NPs) with Ag, Cu, and Mn; one or two metals were used for doping the NPs (seven NP types). First, to synthesize undoped ZnO, a solution containing 100 mL of 0.4 M zinc nitrate hexahydrate ($Zn(NO_3)_2 \cdot 6H_2O$) (119 g/L) and 100 mL of 0.6 M oxalic acid (HO_2CCO_2H) (54.18 g/L) were prepared in deionized water under heating. Then, the oxalic acid solution was slowly added to the ZnO solution, and the sample was placed on a shaker. The resulting solution was stirred for 1 h at 60 °C to 70 °C and finally cooled down at room temperature. Small and even ZnO deposits were washed with distilled water several times. Finally, after 24 h of exposure to ambient air, they were dried in an oven at 100 °C for 5 h [31]. The calcination temperature for the synthesis of ZnO NPs was 450 °C, and the initial pH of solution was 7.0. pH was not measured during the synthesis, which was in accordance with the specific method used by Subash et al. [31].

For the synthesis of Ag-doped ZnO NPs, after preparing the ZnO solution, 5 mL of 0.15 M silver nitrate was added; then, oxalic acid was added, and the synthesis process was repeated similar to undoped NPs. In addition, for the synthesis of Mn-Cu-doped, Ag-Cu-doped, and Ag-Mn-doped ZnO NPs, ZnO solution was first prepared, and then, 0.15 M nitrate silver, 0.397 g of $Mn(CH_3COO)_2 \cdot 4H_2O$, and 0.235 g

Table 1 Structural and physicochemical characteristic of Direct Blue 15 dye

Chemical formula	$C_{34}H_{24}N_6O_{16}S_4Na_4$
Skeletal formula	
3D representation (JSmol)	
Class	Double azo
Hazard class	Health hazard (GHS08)
Hazard and precautionary statements	H350; P201, P202, P281, P308+313, P405, P501
Molecular weight	992.80 g/mol
Solubility in water	Soluble in water 60 g/L (85 °C); insoluble in organic solvents
Appearance (physical description)	Dark blue powder
CAS (Chemical Abstracts Service) number	2429-74-5
European Community (EC) number	219-385-3
PubChem Compound ID	5479507

of $Cu(CH_3COO)_2$ were added. Following that, the oxalic acid solution was added, and the synthesis process was repeated similar to undoped NPs [31]. For the synthesis of all NPs, dopant concentration was 2.5%.

Characterization of nanoparticles

The characteristics of synthesized NPs were determined, based on the scanning electron microscopy (SEM), X-ray diffraction (XRD), Fourier transform infrared (FTIR) spectroscopy, dynamic light scattering (DLS), atomic force microscopy (AFM), and zeta potential

measurements. For this purpose, a TESCAN microscope (model MIRA3, Czech Republic) was used to describe the shape and size of ZnO NPs. On the other hand, XRD analysis was performed to investigate the crystalline structure and network of NPs using an Inel instrument (EQUINOX 3000, France). Also, FTIR spectroscopy of synthesized NPs was carried out using a Bruker Tensor 27 instrument (Germany). To determine the surface morphology of NPs, an AFM microscope (Advance model, Iran) was used. Finally, the size of NPs and zeta potential were measured using a DLS instrument (NanoBrook model, USA).

Analytical methods

The photocatalytic removal of Direct Blue 15 was investigated using ZnO NPs, doped with 2.5% M silver, manganese, and copper, respectively. The sources of UV light included two 30 W lamps (Philips, Netherlands), while sunlight was considered as the source of visible light. In order to compare the photocatalytic activity of undoped NPs and Ag-, Cu-, and Mn-doped NPs, a synthetic dye solution was prepared, containing 1000 mg/L of Direct Blue 15, and used as the standard solution kept at 4 °C.

The experiments were performed in a 250-mL reactor at neutral pH, with an initial dye concentration of 100 mg/L, NP concentration of 2 g/L, and UV light intensity of 30 W, and sunlight was the source of visible light. In this study, two 15-W ultraviolet lamps (UV-C) were used. The distance between the UV lamps and the sample was 10 cm. Temperature control was not necessary because the sample temperature did not change significantly during the process. The samples were placed on a magnetic shaker, which was exposed to a light source for 120 min. At specific intervals, 5 mL of the solution was collected, and absorbance was read after centrifugation, using a UV-Vis spectrophotometer in a wavelength of 585 nm. Then, the percentage of removal efficiency was calculated using the following formula:

$$R = \frac{C_0 - C_e}{C_0} \times 100 \quad (1)$$

where R represents the percentage of dye removal (%), C_0 and C_e denote the initial and the final dye concentration (mg/L), respectively. All experiments were carried out in triplicate. Duplicate experiments in each group were carried out under the same condition, and the mean values were reported.

Results and discussion

Characterization of synthesized nanoparticles

The SEM images of undoped ZnO and Cu-doped ZnO NPs are presented in Fig. 2. The image of undoped ZnO NPs is shown in Fig. 2a. As presented in undoped ZnO image, there are agglomerations and adhesions in these NPs, and particles are not separated. Figure 2b demonstrates Cu-doped ZnO NPs, showing adhesion among particles. Agglomerations and mass formation were observed in these NPs due to their very small size. According to these images, the size of Cu-doped ZnO NPs is smaller than that of undoped ZnO NPs. Moreover, the EDX (energy-dispersive X-ray spectroscopy) images of undoped ZnO and Cu-doped ZnO NPs are shown in Fig. 3. It can be seen that Zn content of undoped ZnO NPs was simultaneously decreased after modification, but Cu content

of Cu-doped ZnO NPs significantly increased from 0 to 3.72 (wt%) which indicated the successful deposition onto ZnO NPs.

In Fig. 4, images of the XRD spectra of undoped ZnO NPs along with Mn-, Ag-, Cu-, Mn-Cu-, Ag-Cu-, and Mn-Ag-doped ZnO NPs are presented. The main seven XRD peaks were identified in (100), (002), (101), (012), (110), (013), and (112) planes, respectively, corresponding to the crystalline structure of ZnO in the Miller index (Joint Committee on Powder Diffraction Standards (JCPDS), No. 36–1451). The sharp peaks indicate the proper crystallization of ZnO NPs. The maximum intensity peak was observed at $2\theta = 37.095^\circ$, corresponding to the (101) plane [32]. The present results of XRD analysis are consistent with similar studies in this area [33, 34].

The FTIR spectra of undoped ZnO NPs along with Ag-Mn-, Ag-Cu-, Mn-Cu, Mn-, Ag-, and Cu-doped ZnO NPs are shown in Fig. 5. This figure shows a strong bond in the wavelength of 469 cm^{-1} , corresponding to the stretching vibration of ZnO NPs [35]. The C=O stretching bond was observed in the wavelength of 1730 cm^{-1} , which is attributed to the presence of organic materials. Also, N-H stretching vibration was seen at 3448 cm^{-1} , which corresponds to N-H stretching bond in amine groups. Mote et al. [36] also reported similar results in an analysis of ZnO NPs doped with chromium oxide. The stretching bond of ZnO NPs was observed in the range of $400\text{--}600 \text{ cm}^{-1}$, while N-H bond was reported at $3400\text{--}3600 \text{ cm}^{-1}$.

In Fig. 6, the AFM images of Cu-doped ZnO NPs are presented. Generally, AFM is a powerful and accurate tool for determining the surface area and size of materials on a nanoscale. The images clearly indicate the uneven surface of Cu-doped NPs. The size of NPs doped with Cu was about 90 nm, respectively, which confirms the results of SEM analysis. Also, in the image, the surface roughness of NPs can be observed due to the uniform distribution of doping agents [37, 38].

Figure 7 presents the distribution of NP size in the aqueous environment, as measured by the DLS technique. Generally, DLS is a useful technique for determining the size of NPs in form of liquid suspensions considering their Brownian motions. The mean NP size was almost 82 nm for both Cu-doped and Ag-doped ZnO NPs, which is slightly different from the results of SEM analysis. This difference can be attributed to the state of agglomeration and NP accumulation in the SEM analysis [39].

Electrostatic zeta potential of nanoparticles was measured using principles of phase analysis light scattering (PALS) and electrophoretic light scattering (ELS), and its result is presented in Table 2 and Fig. 8. Zeta potential plays an important role in determining the stability of dispersed particles in a liquid environment. In aqueous environments with low ionic strength, a zeta potential above 30 mV is adequate to ensure

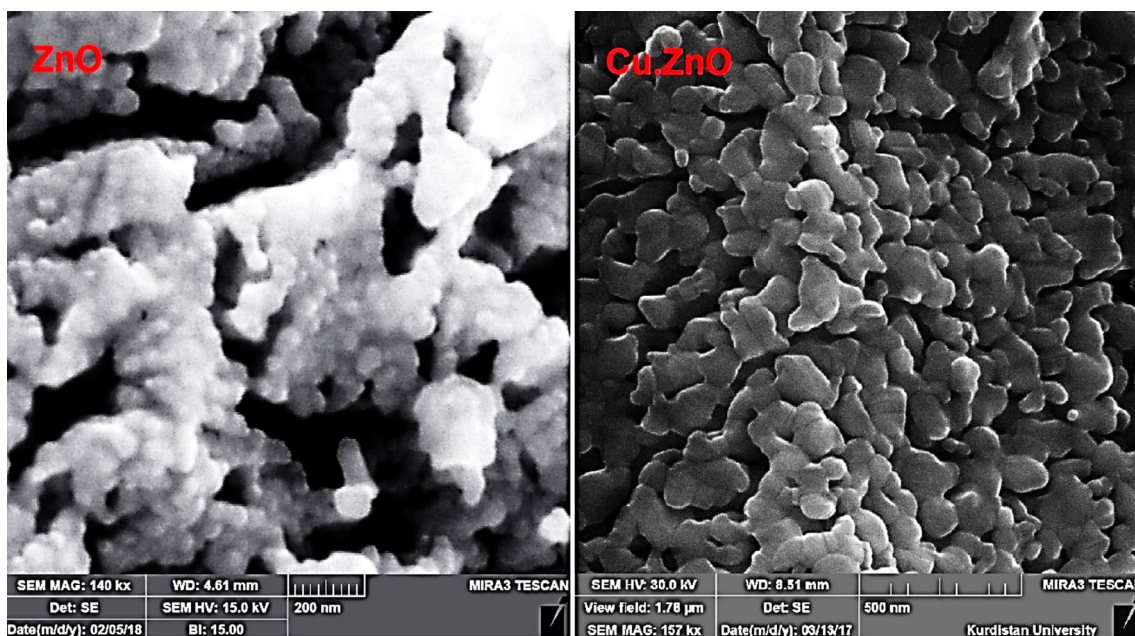


Fig. 2 SEM images and size distribution of **a** undoped ZnO NPs and **b** Cu-doped ZnO NPs

colloidal stability. On the other hand, in aqueous environments containing particles with a low zeta potential, particles have a greater tendency towards agglomeration. In this study, the ionic strength was improved by doping ZnO NPs with transition metals [40].

Effect of transition metals-doped ZnO NPs on dye removal efficiency

ZnO doping with Ag

The photocatalytic decomposition of Direct Blue 15, using undoped, Ag-doped, Ag-Mn-doped, and Ag-Cu-doped ZnO NPs is presented in Fig. 9 under UV and visible light irradiation, respectively. As indicated in Fig. 9, Ag-doped ZnO NPs showed the highest removal efficiency percentage for Direct

Blue 15 under UV radiation within 120 min (73.6%). In comparison with undoped NPs, the improved photocatalytic activity of Ag-doped ZnO NPs under UV radiation could be attributed to the reduced hole-electron recombination due to light exposure on the catalyst surface.

In explanation, as Ag^+ is integrated in the crystalline structure of ZnO NPs, it changes their electron structure. This cation attracts excited electrons from the valence band, prevents the return of electrons, and consequently inhibits the hole-electron recombination in the band. Therefore, free electrons in the conduction band and silver produce more super oxides on the surface of ZnO. On the other hand, the holes exhibit great oxidizing properties and produce hydroxyl radicals by reacting with water molecules. Through greater production of super oxides and radical hydroxyls and prevention of hole-electron recombination, oxidation-regeneration reactions

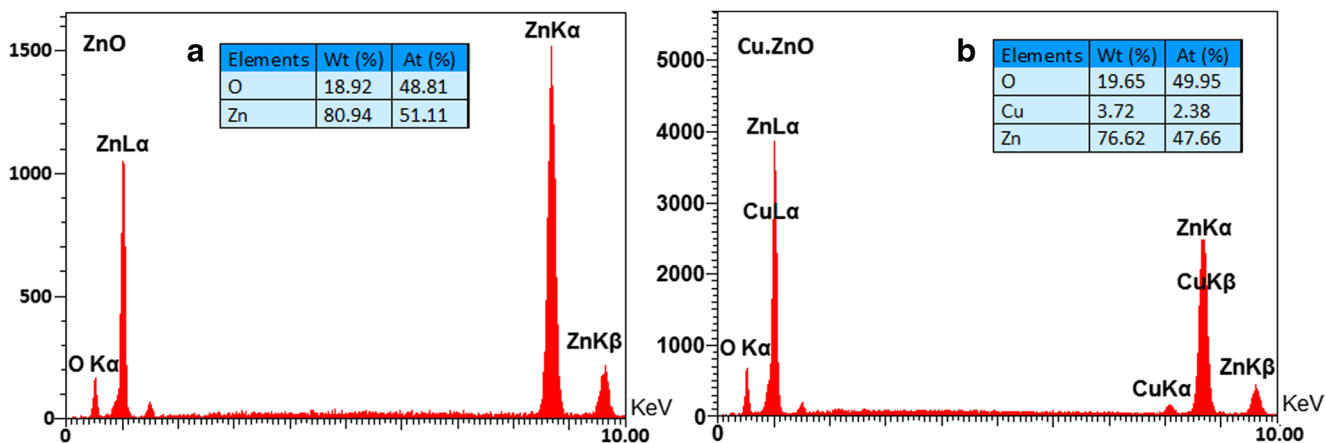


Fig. 3 **a** EDX spectra of undoped ZnO and **b** Cu-doped ZnO NPs

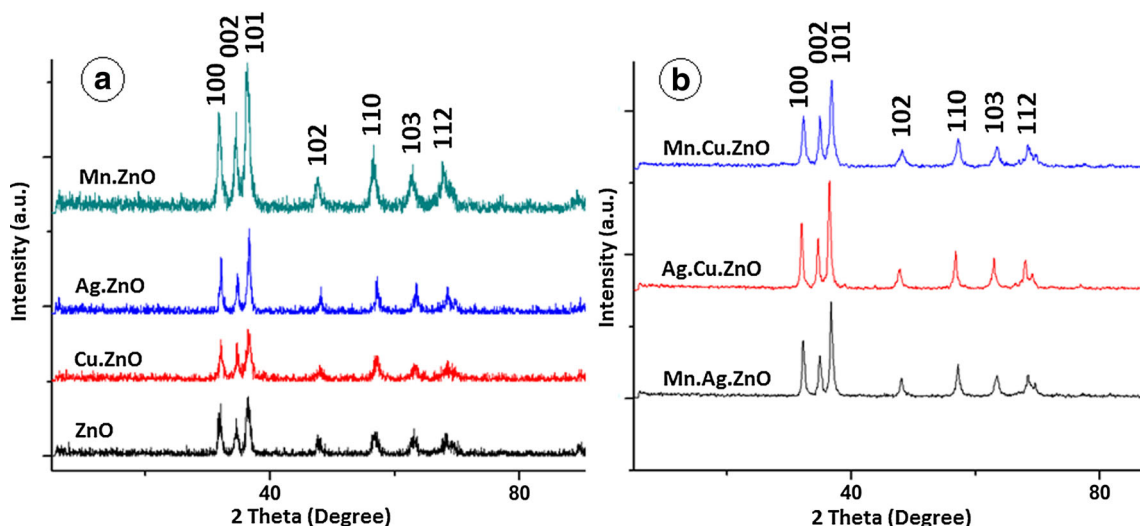


Fig. 4 a XRD diffractograms of undoped ZnO NPs along with Mn-, Ag-, Cu-doped ZnO NPs and b Mn-Cu-, Ag-Cu- and Mn-Ag-doped ZnO NPs

improve, leading to an increase in the removal efficiency of organic dye under UV radiation [21].

The results of a study by Mohammadzadeh et al. [41] on decomposition of Acid Blue 113 by Ag-doped ZnO NPs showed that this catalyst has much greater photocatalytic activities in dye decomposition, compared to undoped ZnO NPs, which is consistent with the results of our study. In addition, Dhatshanamurthi et al. [42] investigated the simultaneous effects of two metals (silver and barium) on the enhanced photocatalytic degradation of azo dye of (Trypan blue) in aqueous solutions using Ba-loaded Ag@ZnO nanocomposite. Their results indicated the greater decomposition of contaminants in the presence of ZnO doped with two metals simultaneously.

Based on the nanophotocatalyst test of ZnO NPs, which were doped with Ag for degradation of Direct Blue 15, dye removal was found to be scarce under visible light (similar

conditions to UV radiation). Since Ag^+ (1.26 Angstrom) has a greater ionic radius than ionized Zn^{2+} (0.74 Angstrom), it is not fully integrated into the ZnO structure. Therefore, the band gap of ZnO is not reduced, and the shift from UV to visible light spectrum is not prominent. In this regard, Bordbar et al. [43] compared the band gap of ZnO doped with three metals, including Ag, Cu, and Cd. It was found that metals with an ionic radius below that of Zn showed a greater reduction in the band gap. In addition, Subash et al. [24] used cerium (Ce)- and Ag-doped ZnO NPs to remove Reactive Red 120 dye, and they reported consistent results with the present study.

ZnO doping with Mn

The photocatalytic degradation of Direct Blue 15 was investigated using undoped, Mn-doped, Ag-Mn-doped, and Mn-Cu-doped ZnO catalysts under UV and visible light radiation; the results are presented in Fig. 10. As can be seen in the figure, the removal efficiency of catalysts was higher under visible light, compared to UV light. The highest removal efficiency under visible light radiation was observed in Ag-Mn-doped ZnO NPs (46.3%).

ZnO doping with Mn and other transition metals can create an intermediate state near the valence band through metal integration in the ZnO structure and consequently reduce the energy gap; the resulting energy gap can extend the light absorption spectrum from UV to visible light. Therefore, at light intensities below UV, electrons are transferred to the intermediate state and conduction band and produce more super oxides and hydroxyl radicals.

Gallegos et al. [44], by analyzing the structural and optical properties of Mn-doped ZnO NPs, showed that the energy gap reduced from 3.3 eV to 3.1 eV, which confirms the results of the present study. Similarly, the results reported by Li et al. [45] showed the high

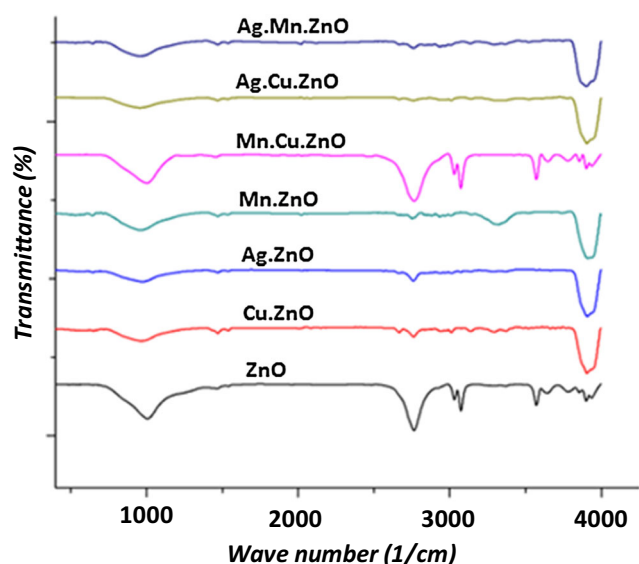


Fig. 5 FTIR diffractograms of undoped ZnO NPs along with Ag-Mn-, Ag-Cu-, Mn-Cu-, Mn-, Ag-, and Cu-doped ZnO NPs

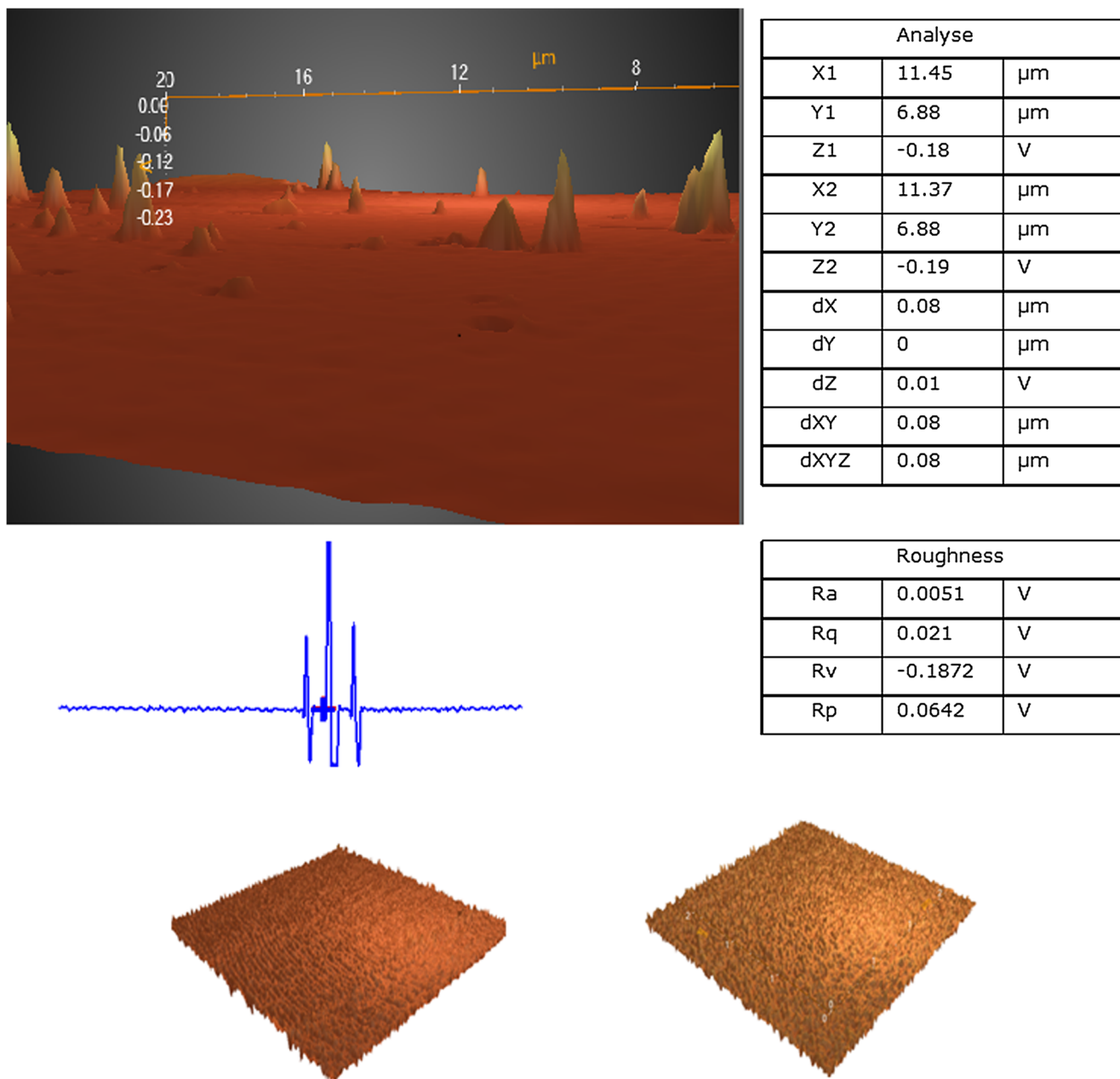


Fig. 6 The AFM images of Cu-doped ZnO NPs

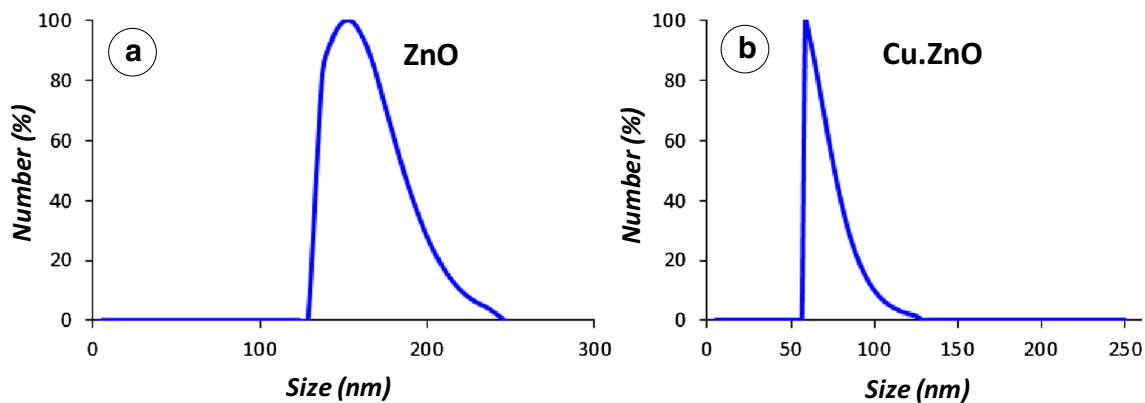


Fig. 7 DLS images of a undoped and b Cu-doped ZnO NPs

Table 2 Zeta potential (PALS^a method) details of undoped and doped (with Cu, Ag, Mn, Cu-Mn, Cu-Ag, and Mn-Ag) ZnO NPs using the Smoluchowski’s model

Sample	Zeta potential (mV)	Mobility ($\mu\text{s}/(\text{V}/\text{cm})$)
ZnO	-10.66	-0.83
Cu.ZnO	-9.71	-0.76
Ag.ZnO	-8.69	-0.68
Mn.ZnO	-12.4	-0.97
Cu.Mn.ZnO	-9.25	-0.72
Cu.Ag.ZnO	-6.81	-0.53
Mn.Ag.ZnO	-3.33	-0.26

^a PALS Phase Analysis Light Scattering

removal efficiency of methyl orange for Mn-doped ZnO, compared to undoped ZnO, which is consistent with our findings. Additionally, Ullah et al. [46] studied and compared the photocatalytic efficiency of Mn-doped and undoped ZnO NPs in the removal of ethylene blue and reported increased dye removal under visible light radiation in the presence of doped ZnO in comparison with undoped ZnO NPs.

ZnO doping with Cu

The analysis of dye removal efficiency by Cu-doped and Ag-Mn-doped ZnO NPs is demonstrated in Fig. 11. Evidently, the

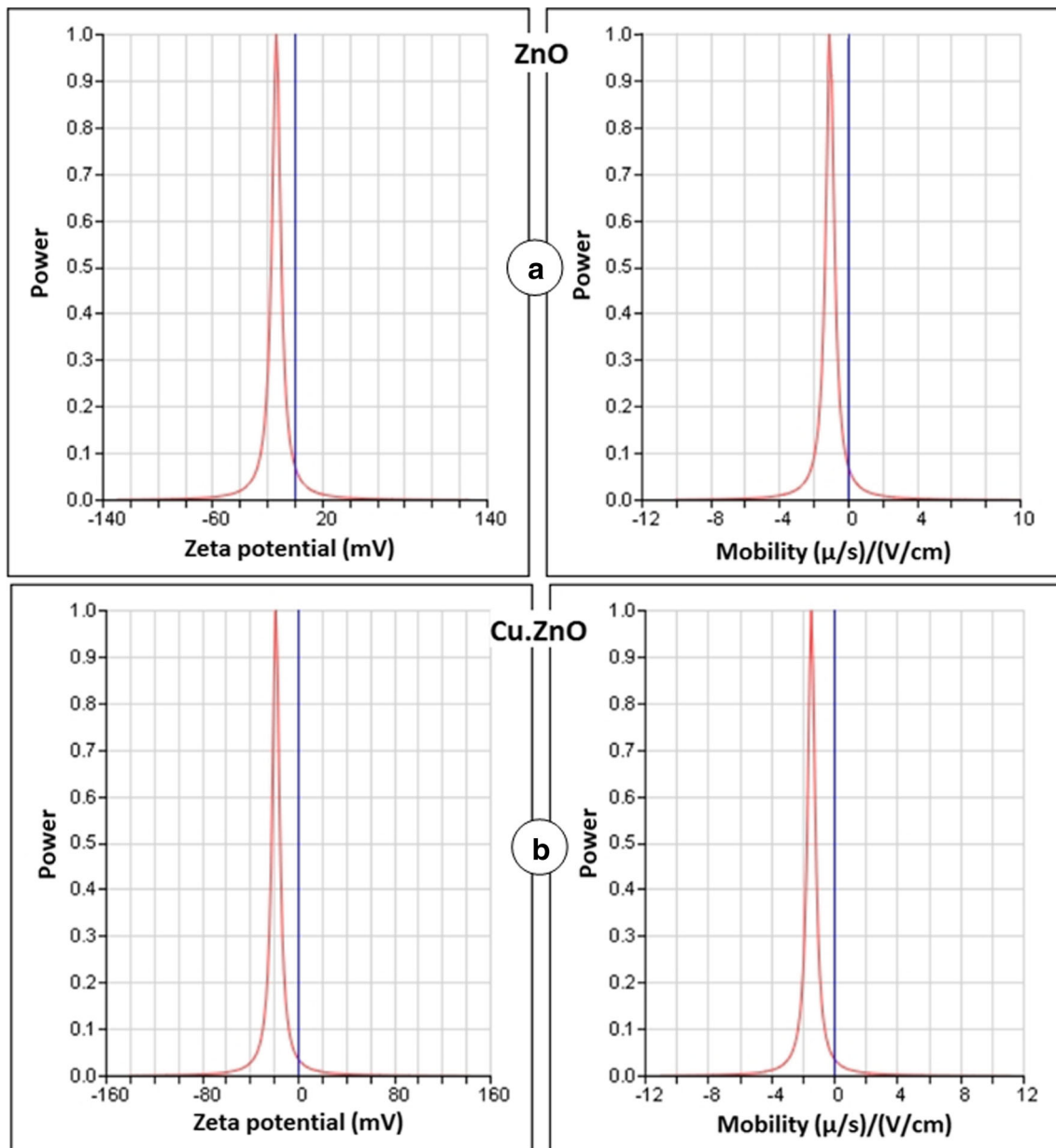
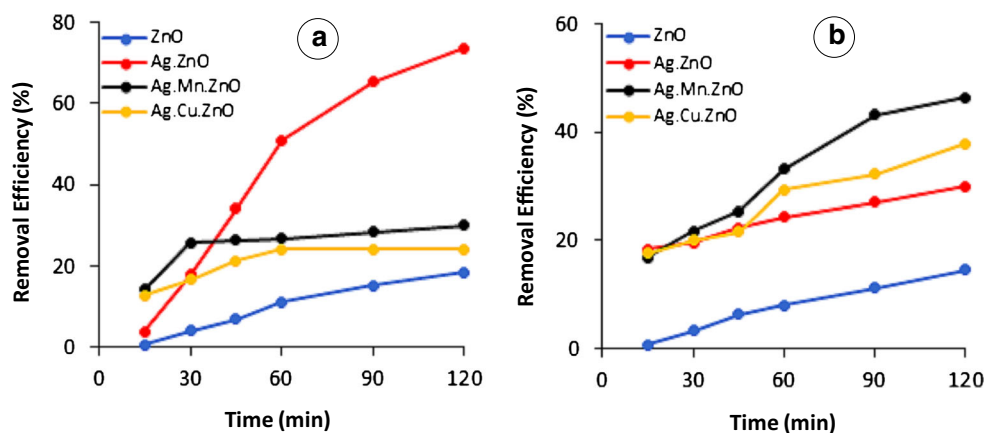


Fig. 8 Zeta potential and mobility (ELS method) of **a** undoped and **b** Cu-doped ZnO NPs

Fig. 9 Effect of different Ag-doped nanophotocatalysts on photocatalytic decomposition of Direct Blue 15 under **a** UV and **b** visible light radiation (initial dye concentration = 100 mg/L, pH = 7; UV intensity = 30 W, and NP concentration = 2 g/L, and dopant percentage = 2.5%)



optical activity of Cu-doped, Ag-Cu-doped, and Mn-Cu-doped ZnO catalysts increased under visible light, compared to UV light radiation. Since the ionic radius of Cu^{2+} (0.73) is smaller than that of Zn (0.74), it can easily penetrate into the crystalline structure of ZnO. Cu increases the luminescence properties of ZnO and causes local impurities in the bond gaps and therefore, resulting the light absorption spectrum shifted to visible light. In addition, Cu^{2+} metal cations act as an electron trap considering the partially filled electron configuration. They also play an important role in reducing hole-electron recombination and increasing the production of oxidizing radicals [47, 48].

A study by Mittal et al. [15] reported an increase in the efficiency of Cu-doped ZnO in comparison with undoped ZnO in crystal violet decomposition due to a shift in absorption towards the visible light spectra. This finding is consistent with the results of our study. Moreover, Sriram et al. [49] found that Cu-doped ZnO nanophotocatalysts exhibited greater photocatalytic activity in methylene blue removal under visible light radiation due to the increased Cu content. In the present study, Ag metal cations had the greatest synergistic

effects on the photocatalytic removal efficiency of Cu-doped ZnO NPs [50].

Comparison of removal efficiency of synthesized nanocatalysts

The results related to the efficiency of seven synthesized nanocatalysts in decomposition of Direct Blue 15 under UV and visible light radiations are presented in Fig. 12, respectively. As shown in these figures, Ag-doped ZnO NPs had the highest efficiency in dye degradation under UV radiation (73.6%), while under similar conditions, a much lower efficiency was reported with visible light radiation (29.96%) for Ag-doped ZnO NPs. Among all synthesized NPs, Cu-doped ZnO NPs exhibited the highest removal efficiency in dye degradation (70%) under visible light irradiation, while under similar conditions Cu-doped ZnO NPs exhibited a lower degradation efficiency about 40% under UV light radiation. According to the results of the experiments and diagrams, other synthesized NPs showed less efficacy in dye degradation under visible light irradiation and UV

Fig. 10 Effect of different Mn-doped nanophotocatalysts on photocatalytic decomposition of Direct Blue 15 under **a** UV and **b** visible light radiation (initial dye concentration = 100 mg/L, pH = 7; UV intensity = 30 W, and NP concentration = 2 g/L, and dopant percentage = 2.5%)

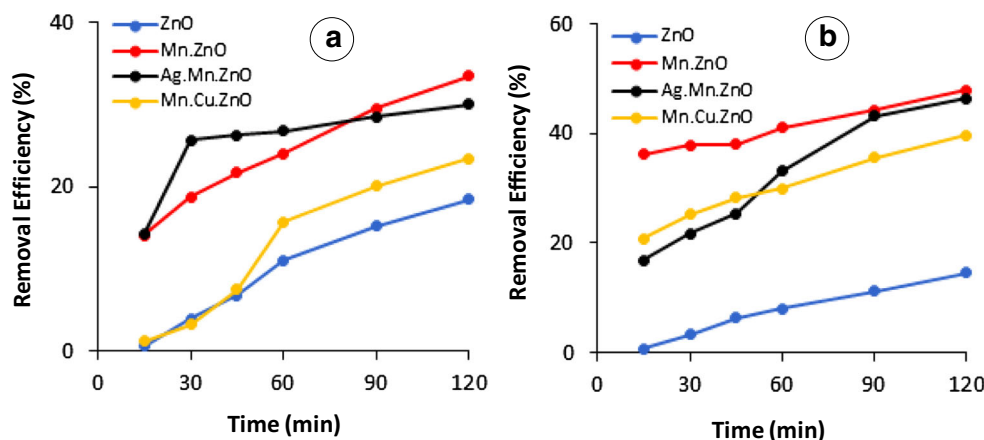
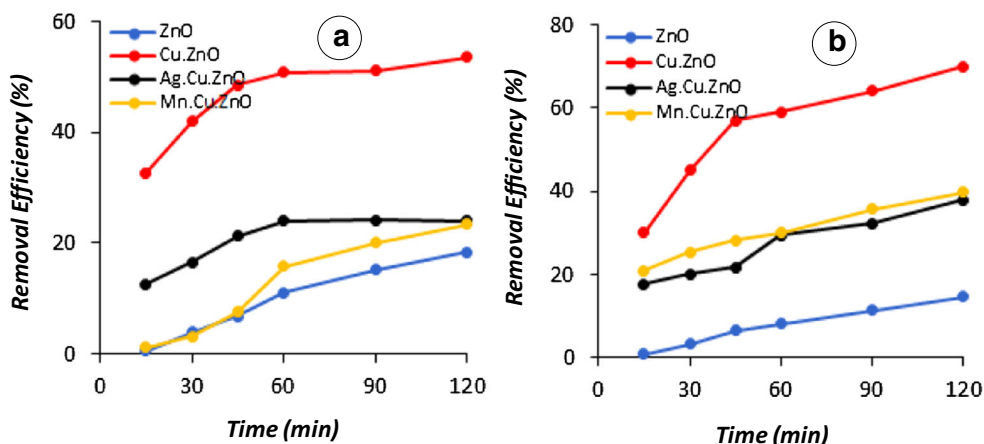


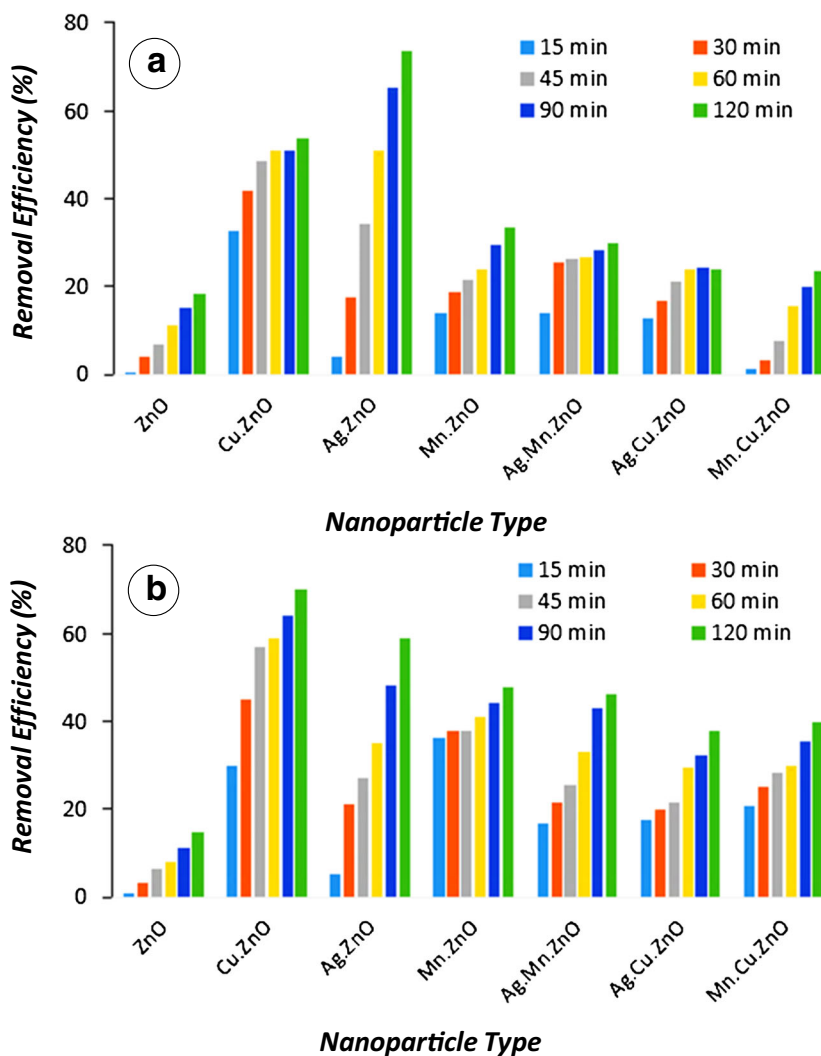
Fig. 11 Effect of different Cu-doped nanophotocatalysts on photocatalytic decomposition of Direct Blue 15 under **a** UV and **b** visible light radiation (initial dye concentration = 100 mg/L, pH = 7; UV intensity = 30 W, and NP concentration = 2 g/L, and dopant percentage = 2.5%)



light radiation. For example, the degradation efficiency of Mn-doped ZnO, Ag-Mn-doped ZnO, Ag-Cu-doped ZnO, and Mn-Cu-doped ZnO NPs under ultraviolet light after 120 min was 33.49, 30, 24, and 23.4%, respectively. For these NPs and under the same conditions, the degradation

efficiency in the presence of visible light irradiation was increased slightly and showed 47.87, 46.31, 37.89 and 39.69% for Mn-doped ZnO, Ag-Mn-doped ZnO, Ag-Cu-doped ZnO, and Mn-Cu-doped ZnO, respectively. Further explanations are needed in this area.

Fig. 12 Efficiency of photocatalytic removal of Direct Blue 15 under **a** UV and **b** visible light radiation



Conclusion

Undoped ZnO NPs along with Mn-, Ag-, Cu-doped ZnO NPs were successfully synthesized using the thermal solvent method for photocatalytic decomposition of Direct Blue 15 under UV radiation and visible light irradiation. The highest removal efficiency under UV radiation was obtained about 74% in the presence of Ag-doped ZnO NPs, while the maximum efficiency under visible light irradiation was achieved as 70% in the existence of Cu-doped ZnO NPs. From practical and economic viewpoints, the efficiency obtained UV radiation was found to be important, and higher removal efficiency values could be achieved by changing the conditions of process-related operating parameters (e.g. pH, light intensity, NP concentration).

The experimental findings revealed that the photocatalytic activity of ZnO NPs in organic dye removal increased after doping with Ag, Mn, and Cu, compared to the undoped state under UV radiation and visible light irradiation. In other words, these results indicated the efficacy of transition metals on reducing the hole-electron recombination, increasing hydroxyl radical ($\bullet\text{OH}$) formation in ZnO, and formation of impurity states in the structure of doped ZnO NPs, which resulted in the increased photocatalytic activity of synthesized NPs. Thus, the synthesis of transition metal-doped ZnO nanophotocatalysts (with one or two metals) under UV radiation or visible light irradiation could be used as an efficient and promising technology for the photocatalytic removal of Direct Blue 15 dye from aqueous environments.

Acknowledgments The authors offer their thanks to the sponsors of the project.

Authors' contributions Designed the study, coordinated all the experiments, participated in manuscript preparation and final approval of the manuscript: AM, KY. Helped in manuscript preparation, data analysis and final approval of the manuscript: RE, BS. Performed laboratory tests, contributed to manuscript preparation and final approval of the manuscript: KH, HD. Contributed to data analysis and interpretation: RG, MS, and RR. Statistical analysis, critical revision: AJ, SHP. All authors reviewed and approved of the final manuscript.

Funding This manuscript is extracted from the project approved by the Environmental Health Research Center and funded by the Kurdistan University of Medical Sciences (IR.MUK.REC.1396/89).

Data availability All the necessary data have been given in the paper. If other investigators need our data for their works, they can contact corresponding authors through the email.

References

- Boumazza S, Kaouah F, Hamane D, Trari M, Omeiri S, Bendjama Z. Visible light assisted decolorization of azo dyes: Direct Red 16 and Direct Blue 71 in aqueous solution on the p-CuFeO₂/n-ZnO system. *J Mol Catal A Chem*. 2014;393:156–65.
- Alvarez LH, Meza-Escalante ER, Gortáres-Moroyoqui P, Morales L, Rosas K, García-Reyes B, et al. Influence of redox mediators and salinity level on the (bio) transformation of Direct Blue 71: kinetics aspects. *J Environ Manag*. 2016;183:84–9.
- Ertugay N, Acar FN. Removal of COD and color from Direct Blue 71 azo dye wastewater by Fenton's oxidation: kinetic study. *Arab J Chem*. 2013;10:1158–63.
- Saien J, Soleymani A. Degradation and mineralization of Direct Blue 71 in a circulating upflow reactor by UV/TiO₂ process and employing a new method in kinetic study. *J Hazard Mater*. 2007;144:506–12.
- Zandsalimi Y, Taimori P, Soltani RDC, Rezaee R, Abdullahi N, Safari M. Photocatalytic removal of acid red 88 dye using zinc oxide nanoparticles fixed on glass plates. *J Adv Environ Health Res*. 2015;3:102–10.
- Shirmardi M, Mahvi AH, Mesdaghinia A, Nasser S, Nabizadeh R. Adsorption of acid red 18 dye from aqueous solution using single-wall carbon nanotubes: kinetic and equilibrium. *Desalin Water Treat*. 2013;51(34–36):6507–16.
- Nadafi K, Vosoughi M, Asadi A, Borna MO, Shirmardi M. Reactive Red 120 dye removal from aqueous solution by adsorption on nano-alumina. *J Water Chem Technol*. 2014;36(3):125–33.
- Shirmardi M, Mesdaghinia A, Mahvi AH, Nasser S, Nabizadeh R. Kinetics and equilibrium studies on adsorption of acid red 18 (Azo-Dye) using multiwall carbon nanotubes (MWCNTs) from aqueous solution. *J Chem*. 2012;9(4):2371–83.
- Konicki W, Sibera D, Mijowska E, Lendzion-Bieluń Z, Narkiewicz U. Equilibrium and kinetic studies on acid dye Acid Red 88 adsorption by magnetic ZnFe₂O₄ spinel ferrite nanoparticles. *J Colloid Interface Sci*. 2013;398:152–60.
- Shahmoradi B, Negahdary M, Maleki A. Hydrothermal synthesis of surface-modified, manganese-doped TiO₂ nanoparticles for photodegradation of methylene blue. *Environ Eng Sci*. 2012;29(11):1032–7.
- Mozia S, Tomaszewska M, Morawski AW. Photocatalytic degradation of azo-dye acid red 18. *Desalination*. 2005;185(1–3):449–56.
- Sathishkumar P, Pugazhentiran N, Mangalaraja RV, Asiri AM, Anandan S. ZnO supported CoFe₂O₄ nanophotocatalysts for the mineralization of Direct Blue 71 in aqueous environments. *J Hazard Mater*. 2013;252:171–9.
- Ajmal A, Majeed I, Malik R, Iqbal M, Nadeem MA, Hussain I, et al. Photocatalytic degradation of textile dyes on Cu₂O-CuO/TiO₂ anatase powders. *J Environ Chem Eng*. 2016;4(2):2138–46.
- Ghaneian MT, Morovati P, Ehrampoush MH, Tabatabaee M. Humic acid degradation by the synthesized flower-like Ag/ZnO nanostructure as an efficient photocatalyst. *J Environ Health Sci Eng*. 2014;12:138.
- Zhou K, Hu X-Y, Chen B-Y, Hsueh C-C, Zhang Q, Wang J, et al. Synthesized TiO₂/ZSM-5 composites used for the photocatalytic degradation of azo dye: intermediates, reaction pathway, mechanism and bio-toxicity. *Appl Surf Sci*. 2016;383:300–9.
- Mittal M, Sharma M, Pandey OP. UV-visible light induced photocatalytic studies of Cu doped ZnO nanoparticles prepared by coprecipitation method. *Sol Energy*. 2014;110:386–97.
- Karimi L, Zohoori S, Yazdandehnas ME. Photocatalytic degradation of azo dyes in aqueous solutions under UV irradiation using nano-strontium titanate as the nanophotocatalyst. *J Saudi Chem Soc*. 2014;18(5):581–8.
- Hadi M, McKay G, Samarghandi MR, Maleki A, Solaimany Aminabad M. Prediction of optimum adsorption isotherm: comparison of chi-square and log-likelihood statistics. *Desalin Water Treat*. 2012;49(1–3):81–94.
- Senthilraja A, Subash B, Krishnakumar B, Rajamanickam D, Swaminathan M, Shanthi M. Synthesis, characterization and catalytic activity of co-doped Ag–Au–ZnO for MB dye degradation under UV-A light. *Mater Sci Semicond Process*. 2014;22:83–91.

20. Muhd Julkapli N, Bagheri S, Bee Abd Hamid S. Recent advances in heterogeneous photocatalytic decolorization of synthetic dyes. *Sci World J.* 2014;692307:1–25.
21. Samadi M, Zirak M, Naseri A, Khorashadizade E, Moshfegh AZ. Recent progress on doped ZnO nanostructures for visible-light photocatalysis. *Thin Solid Films.* 2016;605:2–19.
22. Elias M, Amin MK, Firoz SH, Hossain MA, Akter S, Hossain MA, et al. Microwave-assisted synthesis of Ce-doped ZnO/CNT composite with enhanced photo-catalytic activity. *Ceram Int.* 2017;43:84–91.
23. Xu C, Cao L, Su G, Liu W, Qu X, Yu Y. Preparation, characterization and photocatalytic activity of Co-doped ZnO powders. *J Alloys Compd.* 2010;497(1–2):373–6.
24. Subash B, Krishnakumar B, Swaminathan M, Shanthi M. Synthesis and characterization of cerium–silver co-doped zinc oxide as a novel sunlight-driven photocatalyst for effective degradation of reactive Red 120 dye. *Mater Sci Semicond Process.* 2013;16(4):1070–8.
25. Soltani RDC, Jorfi S, Ramezani H, Purfadakari S. Ultrasonically induced ZnO–biosilica nanocomposite for degradation of a textile dye in aqueous phase. *Ultrason Sonochem.* 2016;28:69–78.
26. Mekasuwandumrong O, Pawinrat P, Praserttham P, Panpranot J. Effects of synthesis conditions and annealing post-treatment on the photocatalytic activities of ZnO nanoparticles in the degradation of methylene blue dye. *Chem Eng J.* 2010;164(1):77–84.
27. Maleki A, Shahmoradi B. Solar degradation of Direct Blue 71 using surface modified iron doped ZnO hybrid nanomaterials. *Water Sci Technol.* 2012;65(11):1923–8.
28. Palmisano L, Augugliaro V, Sclafani A, Schiavello M. Activity of chromium-ion-doped titania for the dinitrogen photoreduction to ammonia and for the phenol photodegradation. *J Phys Chem.* 1988;92(23):6710–3.
29. Kumar R, Umar A, Kumar G, Akhtar MS, Wang Y, Kim SH. Ce-doped ZnO nanoparticles for efficient photocatalytic degradation of direct red-23 dye. *Ceram Int.* 2015;41(6):7773–82.
30. Chang CJ, Lin CY, Hsu MH. Enhanced photocatalytic activity of Ce-doped ZnO nanorods under UV and visible light. *J Taiwan Inst Chem Eng.* 2014;45(4):1954–63.
31. Subash B, Krishnakumar B, Velmurugan R, Swaminathan M, Shanthi M. Synthesis of Ce co-doped Ag–ZnO photocatalyst with excellent performance for NBB dye degradation under natural sunlight illumination. *Cat Sci Technol.* 2012;2(11):2319–26.
32. Sowa H, Ahsbahs H. High-pressure X-ray investigation of zincite ZnO single crystals using diamond anvils with an improved shape. *J Appl Crystallogr.* 2006;39(2):169–75.
33. Kathirvel P, Manoharan D, Mohan SM, Kumar S. Spectral investigations of chemical bath deposited zinc oxide thin films–ammonia gas sensor. *J Optoelectron Biomed Mater.* 2009;1:25–33.
34. Shirmardi M, Alavi N, Lima EC, Takdastan A, Mahvi AH, Babaei AA. Removal of atrazine as an organic micro-pollutant from aqueous solutions: a comparative study. *Process Saf Environ Prot.* 2016;103:23–35.
35. Kwon YJ, Kim KH, Lim CS. Characterization of ZnO nanoparticles synthesized by the polymerized complex method via an organochemical route. *J Ceram Process Res.* 2002;3(3):146–9.
36. Mote VD, Huse VR, Dole BN. Synthesis and characterization of Cr doped ZnO nanocrystals. *World J Condens Matter Phys.* 2012;2(2):208–11.
37. Joshi K, Rawat M, Gautam SK, Singh RG, Ramola RC, Singh F. Band gap widening and narrowing in Cu-doped ZnO thin films. *J Alloys Compd.* 2016;680:252–8.
38. Wang R, Xin JH, Yang Y, Liu H, Xu L, Hu J. The characteristics and photocatalytic activities of silver doped ZnO nanocrystallites. *Appl Surf Sci.* 2004;227(1–4):312–7.
39. Shyni LS, Jagadish K, Srikantaswamy S, Abhilash M. Photocatalytic degradation and removal of heavy metals in pharmaceutical waste by selenium doped ZnO nano composite semiconductor. *J For Res.* 2016;2(5):47–54.
40. Suganthi KS, Rajan KS. Temperature induced changes in ZnO–water nanofluid: zeta potential, size distribution and viscosity profiles. *Int J Heat Mass Transf.* 2012;55(25–26):7969–80.
41. Mohammadzadeh S, Olya ME, Arabi AM, Shariati A, Nikou MK. Synthesis, characterization and application of ZnO–Ag as a nanophotocatalyst for organic compounds degradation, mechanism and economic study. *J Environ Sci.* 2015;35:194–207.
42. Dhathshanamurthi P, Shanthi M. Enhanced photocatalytic degradation of azo dye in aqueous solutions using Ba@ Ag@ ZnO nanocomposite for self-sensitized under sunshine irradiation. *Int J Hydrog Energy.* 2017;42(8):5523–36.
43. Bordbar M, Khodadadi B, Mollatayefe N, Yeganeh FA. Influence of metal (Ag, Cd, Cu)-doping on the optical properties of ZnO nanopowder: variation of band gap. *J Appl Chem.* 2013;8(27):43–8.
44. Gallegos MV, Peluso MA, Thomas H, Damonte LC, Sambeth JE. Structural and optical properties of ZnO and manganese-doped ZnO. *J Alloys Compd.* 2016;689:416–24.
45. Li W, Wang G, Chen C, Liao J, Li Z. Enhanced visible light photocatalytic activity of ZnO nanowires doped with Mn²⁺ and Co²⁺ ions. *Nanomaterials.* 2017;7(1):1–11.
46. Ullah R, Dutta J. Photocatalytic degradation of organic dyes with manganese-doped ZnO nanoparticles. *J Hazard Mater.* 2008;156(1–3):194–200.
47. Polat İ, Yılmaz S, Altın İ, Bacaksız E, Sökmen M. The influence of Cu-doping on structural, optical and photocatalytic properties of ZnO nanorods. *Mater Chem Phys.* 2014;148(3):528–32.
48. Mohan R, Krishnamoorthy K, Kim SJ. Enhanced photocatalytic activity of Cu-doped ZnO nanorods. *Solid State Commun.* 2012;152(5):375–80.
49. Sriram S, Lalithambika KC, Thayumanavan A. Experimental and theoretical investigations of photocatalytic activity of Cu doped ZnO nanoparticles. *Optik.* 2017;139:299–308.
50. Wang YY, Xie H, Zhang W, Tang YB, Chen FY. Preparation and photocatalytic activity of Fe–Ce–N tri-doped TiO₂ catalysts. *Adv Mater Res.* 2013;750–752:1276–82.

Publisher's note Springer Nature remains neutral with regard to jurisdictional claims in published maps and institutional affiliations.

Affiliations

Roya Ebrahimi¹ · Khosro Hossienzadeh¹ · Afshin Maleki¹ · Reza Ghanbari² · Reza Rezaee¹ · Mahdi Safari¹ · Behzad Shahmoradi¹ · Hiua Daraei¹ · Ali Jafari³ · Kaan Yetilmezsoy⁴  · Shivaraju Harikaranahalli Puttaiah⁵

¹ Environmental Health Research Center, Research Institute for Health Development, Kurdistan University of Medical Sciences, Sanandaj, Iran

² Social Determinant of Health Research, Qazvin University of Medical Sciences, Qazvin, Iran

³ School of Health, Lorestan University of Medical Sciences, Khorramabad, Iran

⁴ Department of Environmental Engineering, Faculty of Civil Engineering, Yildiz Technical University, Davutpasa Campus, 34220 Esenler, Istanbul, Turkey

⁵ Department of Water and Health, Faculty of Life Sciences, Jagadguru Sri Shivarathreeshwara University, Sri Shivarathreeshwara Nagara, Mysuru, Karnataka 570015, India